

Molecular Physics



An International Journal at the Interface Between Chemistry and Physics

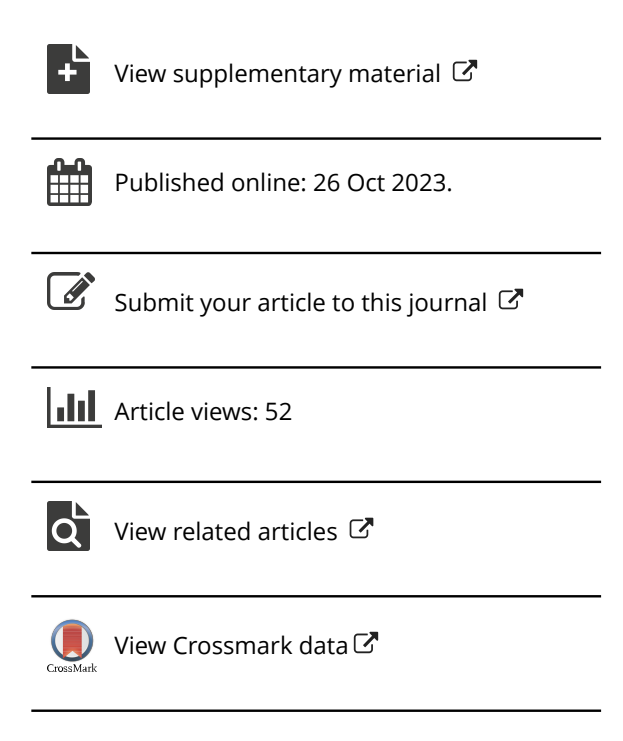
ISSN: (Print) (Online) Journal homepage: www.tandfonline.com/journals/tmph20

Ab initio calculations of through-space and through-bond charge-transfer properties of interacting Janus-like PbSe and CdSe quantum dot heterostructures

Hadassah B. Griffin, Andrei B. Kryjevski & Dmitri S. Kilin

To cite this article: Hadassah B. Griffin, Andrei B. Kryjevski & Dmitri S. Kilin (26 Oct 2023): *Ab initio* calculations of through-space and through-bond charge-transfer properties of interacting Janus-like PbSe and CdSe quantum dot heterostructures, Molecular Physics, DOI: 10.1080/00268976.2023.2273415

To link to this article: https://doi.org/10.1080/00268976.2023.2273415





2023 SANIBEL PROCEEDINGS



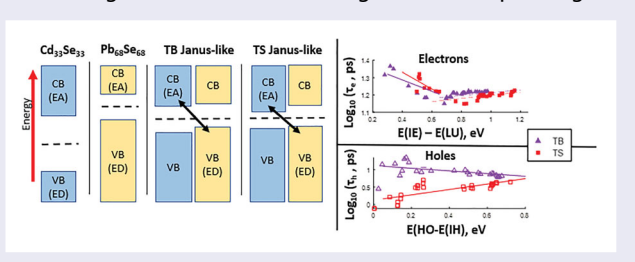
Ab initio calculations of through-space and through-bond charge-transfer properties of interacting Janus-like PbSe and CdSe quantum dot heterostructures

Hadassah B. Griffin^a, Andrei B. Kryjevski^a and Dmitri S. Kilin ⁶

^aDepartment of Physics, North Dakota State University, Fargo, ND, USA; ^bDepartment of Chemistry and Biochemistry, North Dakota State University, Fargo, ND, USA

ABSTRACT

Heterostructure quantum dots (QDs) are composed of two QD nanocrystals (NCs) conjoined at an interface. They are useful in applications such as photovoltaic solar cells. The properties of the interface between the NCs determine the efficiency of electron–hole recombination rates and charge transfer. Therefore, a fundamental understanding of how this interface works between the two materials is useful. To contribute to this understanding, we simulated two isolated heterostructure QD models with Janus-like geometry composed of $Cd_{33}Se_{33} + Pb_{68}Se_{68}$ NCs. The first Janus-like model has a bond connection between the two NCs and is approximately $16 \times 17 \times 29 \text{ Å}^3$ in size. The second model has a through-space connection between the NCs and is approximately $16 \times 17 \times 31 \text{ Å}^3$. We use density functional theory to simulate the ground state properties of these models. Nonadiabatic on-the-fly couplings calculations were then used to construct the Redfield Tensor, which described the excited state dynamics due to nonradiative relaxation. From our results, we identified a qualitative trend which shows that having a bond connecting the two NCs reduces hole relaxation time. We also identified for a sample of electron–hole excitations pairs that the through-bond model allows for a net positive or negative numerical net charge transfer, depending on the excitation pair.



ARTICLE HISTORY

Received 1 May 2023 Accepted 17 October 2023

KEYWORDS

Nonadiabatic couplings; Redfield tensor; heterostructure quantum dots; solar cells; nonradiative relaxation

Introduction

Quantum dots (QDs) have unique electrical properties such as high quantum yield [1,2], multiple exciton generation (MEG) rates [3,4], tunable absorption and emission spectra that can cover the entire visible spectrum [5,6], and tunable band alignment for relaxation pathways of photogenerated carriers [7,8]. These properties are useful for devices such as solar cells [1,3,9]. To better understand these properties, and possibly improve them, computational simulations of QDs can be performed.

A QD's ability to transfer charge is one of its dynamic electric properties that is especially relevant in photovoltaic applications [10]. Various studies have analysed how different aspects of QDs affect charge transfer. The impact of a QD's geometry on charge transfer,

including heterostructure core–shell QD [2,4,11,12] and heterostructure Janus QD [1,3,4,8] configurations, has been explored. In this paper, we classify a Janus QD as a structure with two nanocrystal (NC) hemispheres conjoined at an interface. The types of NCs that can be used to compose these heterostructure models include PbSe and CdSe, whose individual QD properties have been studied extensively in *ab initio* [13–15] and experimental studies [1,16].

While core-shell and Janus QD geometries have both been shown to slow charge carrier cooling and have high MEG rates, the Janus QD geometry allows for both electron and hole photogenerated carriers to be extracted. This accessibility is important for redirecting these carriers to other MEG relaxation pathways, which in turn can be useful when constructing photoconductive devices [3].

Previous studies have also focused on how charge transfer is affected by choice of material in the NCs [4]. The charge transfer properties can also be impacted by a substrate connected to different parts of the interface [13,17]. Changing the stoichiometry of the QDs also impacts charge transfer [8]. The effect of changing the net charge on clusters of multiple QDs has been the subject of an *ab initio* study of PbS NCs [18].

A less explored aspect of heterostructure QD charge transfer is the impact of having a through-bond (TB) versus through-space (TS) connection between the interface of the NCs composing the heterostructure. An *ab initio* investigation of bond connection and interface properties has been done previously for doped silicon QDs [19]. Another recent ab initio study investigated the effect of twisting epitaxially fused ZnTe/ZnSe QD heterodimers on the generation of charge transfer excitons [20]. An experiment investigated the changes in absorption spectra for fused or separated core–shell CdSe/CdS QD dimers [12]. TB and TS studies have also been done for non-QD structures such as thermally activated delayed fluorescence emitters molecular systems [21].

The dynamic information for optoelectronic information in similar classes of QD models can be obtained by a variety of computational methods. These include explicitly correlated Hartree-Fock Method [22], coupled cluster theory [23], diffusion Monte Carlo quantum methods [24], and the GW/BSE approach [15,25], surface hopping [26,27], and multiple spawning [28,29]. Nonadiabatic coupling (NAC) calculations, also known as electron phonon couplings, have recently been calculated by applying machine learning techniques [30,31]. One of the practical and efficient options for obtaining optoelectronic information is calculating on-the-fly NAC calculations and then constructing the Redfield Tensor based on NAC results. The Redfield Tensor contains information about how the photoexcited charge carrier densities change over time as a system relaxes toward thermal equilibrium [10,32].

In our study, we used on-the-fly NAC and the Redfield Tensor to study how the nonradiative relaxation rates and the charge transfer between the interfaces of a Janus-like QD composed of $Pb_{68}Se_{68} + Cd_{33}Se_{33}$ is impacted by TS or TB connection between the interfaces of the two NCs. A Janus-like QD contains two nearly spherical NCs that are in close physical proximity to each other. Special features of true Janus QDs can be understood by analysing limiting cases such as this Janus-like configuration. We examined the case of independent PbSe and CdSe QDs and a Janus-like QD with a TS connection. We compared

these models, with a focus on the Janus-like TS model, with the case of the NCs in a Janus-like formation with a TB connection. Our chosen QD geometry is unique compared to core–shell and Janus QD models since our main NC components have little contact with their heterostructure counterparts. This minimal contact allows us to examine in greater detail the impact of TB versus TS connection between NCs on nonradiative relaxation rates and charge transfer.

We hypothesised that a TB connection would slow the relaxation rates of charge carriers in the Janus-like QDs because this slowing of rates has previously been observed in Janus QDs [3]. We also hypothesised that having a TB or TS connection would have an impact on the observed charge transfer during the relaxation process. To prove this, we examined ground and dynamic states for both models.

In the following sections, we give more details about the theory behind our ground and dynamic state analysis. We present the results of both analyses. With regards to dynamic results, we identified two significant qualitative differences between the TB and TS Janus-like models. First, the hole relaxation for the TB model does not follow the energy gap law for semiconductors [33]; instead, its relaxation rate increases as the energy gap increases. The hole relaxations for the TB model also take a longer time to occur than the TS model relaxations in general, which is beneficial for applications like harvesting charged particles in solar cells [3]. The second significant qualitative difference we found was that the TB model allowed for a numerical net positive or negative charge transfer during nonradiative relaxation for a sample of electron-hole relaxation pairs, while the TS model mostly favoured a net negative charge transfer.

Methods

Ground state calculations

In order to analyse the ground state properties of the Janus-like models and their individual NC counterparts, we applied density functional theory (DFT) [34] (Supplemental Information 1).

Notations for positions of ions, Kohn–Sham (KS) orbitals, and KS energies are defined in Supplemental Equation S1. Once we have the ground state energies from solving Supplemental Equation S1, [35] we then can determine the band gap of our given model by evaluating the difference in energy of the highest occupied KS molecular orbital (HOMO) and lowest occupied KS molecular orbital (LUMO):

$$E_g(KS) = E_g - \Delta xc = \varepsilon_{n+1}(KS) - \varepsilon_n(KS)$$
 (1a)

In Equation (1), Δxc is the difference between the energies of the $(n+1)_{th}$ orbitals of the KS systems. This difference is given by the KS orbitals that correspond to the ionised and neutral electron systems. Another item of note is that the excited states of our system that are used to construct our density matrices can be represented as a superposition of electron-hole pairs:

$$|\psi_{\alpha}\rangle = \sum_{eh} A_{eh}^{\alpha} |\varphi_{e}^{KS}\rangle \otimes |\varphi_{h}^{KS}\rangle$$
 (1b)

One may assume that there is a leading order term in the expansion coefficient:

$$A_{eh}^{\alpha} = \delta_{ee'}\delta_{hh'} + O^2 \tag{1c}$$

Under this approximation, a single pair of noninteracting *e*' and *h*' can represent an excited state.

We also examined the absorption spectra of our four models. In order to obtain these, we need the dipole oscillator strength \vec{D}_{ij} to get the absorption rate f_{ij} : [32].

$$f_{ij} = \frac{4\pi \, m_e \omega_{ij}}{3he^2} |\vec{D}_{ij}|^2 \tag{2}$$

where m_e is the mass of an electron, e is the charge of an electron, and:

$$\omega_{ij} = \frac{\varepsilon_i - \varepsilon_j}{\hbar} \tag{3}$$

is the angular frequency required to excite an electron from a state *i* to a state *j*. The transition dipole moment from a state *i* to *j* is:

$$\vec{D}_{ij} = e \int d\vec{r} \varphi_i^{KS*}(\vec{r}) \cdot \vec{r} \cdot \varphi_j^{KS}(\vec{r})$$
 (4)

Here $\varphi_i^{\text{KS}}(\vec{r})$ is a KS orbital found while solving Supplemental Equation S1. Once the absorption rates are calculated, one can plot the spectral density of absorption by using the following equation:

$$\alpha(\omega) = \sum_{i \le HO} \sum_{j \ge LU} f_{ij} \delta(\hbar \omega - \hbar \omega_{ij})$$
 (5)

Dynamic calculations

A critical step in moving forward with dynamic calculations is subjecting our model to a thermal bath which drives it away from equilibrium. Once a system is thermally excited, we perform molecular dynamic (MD) microcanonical ensemble simulations to create a trajectory of the system state over time. The positions of ions $\vec{R}_i = \vec{R}_i(t)$, KS energies $\varepsilon_i = \varepsilon_i(\{\vec{R}_i(t)\})$, and KS orbitals $\varphi_i^{KS} = \varphi_i^{KS}(\overrightarrow{r}, \{\overrightarrow{R}_i(t)\})$ become time-dependent and allow consideration beyond Born-Oppenheimer approximation. The information from the MD steps can be used to calculate on-the-fly NAC, which are used to construct the Redfield Tensor, for a perturbative account of electron-to-nuclear interaction [10,32]. In order to implement NAC, we calculate the coupling between states i and j at two different times steps in a given trajectory:

$$V_{ij}^{NA}(t) = -\frac{i\hbar}{2\Delta t} \int d\vec{r} \varphi_i^{KS*}(\vec{r}, \{\vec{R}_i(t)\}) \varphi_j^{KS} \times (\vec{r}, \{\vec{R}_i(t + \Delta t)\}) + h.c.$$
 (6)

A set of couplings is then entered into the autocorrelation function:

$$M_{ijkl}(\tau) = \frac{1}{T} \int_0^T V_{ij}(t+\tau) V_{kl}(t) dt$$
 (7)

Here T is the total time span of the trajectory. We then take a Fourier Transform of Equation (7) to get its partial components:

$$\Gamma_{ljik}^{+} = \int d\tau M_{ljik}(\tau) \exp(-i\omega_{ik}\tau)$$
 (8)

$$\Gamma_{ljik}^{-} = \int d\tau M_{ljik}(\tau) \exp(-i\omega_{lj}\tau)$$
 (9)

Equations (8) and (9) can be used to construct the Redfield Tensor, which controls the density matrix ρ_{ik} dynamics of a system:

$$R_{ijkl} = \Gamma_{ijkl}^{-} + \Gamma_{ijkl}^{+} + \delta_{lj} \sum_{m} \Gamma_{ijkl}^{+} - \delta_{ik} \sum_{m} \Gamma_{ijkl}^{-} \quad (10)$$

$$\left(\frac{d\rho_{jk}}{dt}\right)_{diss} = \sum_{lm} R_{jklm} \rho_{lm} \tag{11}$$

Suppose our system is now stimulated by a photon. There is an excitation energy between a state A and B:

$$\hbar\Omega_{AB} = E_{A\to B}^{tot} - E_{ground}^{tot} \approx \varepsilon_A - \varepsilon_B$$
 (12)

In terms of our density matrix, at time t = 0, we can define our excitation energy as:

$$\rho_{ij}(0) = \delta_{ij}(f_i - \delta_{iA} + \delta_{jB}) \tag{13}$$

here f_i is the Fermi Dirac thermal population of state i. We then solve the equations of motion in order to find the time evolution of our electronic state:

$$\rho_{ij} = -\frac{i}{\hbar} \sum_{k} (F_{ik} \rho_{kj} - \rho_{jk} F_{ki}) + \left(\frac{d\rho_{ij}}{dt}\right)_{diss}$$
(14)

Here F_{ki} represents the matrix element of the KS state term, which comes from the dissipation energy of electronic to nuclear degrees of freedom. The numerical solutions of the autocorrelation function (Equation (7)) give the time-dependent elements of the density matrix $\rho_{ik}(t)$. These functions can describe electron and hole state dynamics.

Now that we can solve our density matrix, we can calculate observables using Equation (10). We also can describe the time-dependent occupation values of the KS states with the diagonal elements of the density matrix ρ_{ii} . By knowing dissipation rates and occupation values, we can calculate charge distribution dynamics, energy dissipation rates, and charge transfer rates.

We can express our charge distribution as an equilibrium distribution:

$$n(\varepsilon, t) = \sum_{i} \rho_{ii}(t)\delta(\varepsilon - \varepsilon_i)$$
 (15)

Our change of charge distribution, or population dynamics, can then be expressed as:

$$\Delta n(\varepsilon, t) = n(\varepsilon, t) - n(\varepsilon) \tag{16}$$

When $\Delta n > 0$ in Equation (16), there is a population gain which corresponds to the electron part of an excitation occurring at energy ε . When $\Delta n < 0$, we have a population loss which corresponds to a hole excitation at the energy ε . We can calculate the expectation energy of our charge carrier with:

$$\langle \Delta \varepsilon_{e/h} \rangle (t) = \sum_{i} \rho_{ii}(t) \varepsilon_{i}(t)$$
 (17)

As is typical for white noise-driven dissipative systems, it is reasonable to assume that our energy dissipation can be written as an exponential. We can then describe the relaxation rate *k* of electrons and holes as follows:

$$k_{e/h} = \{\tau^{e/h}\}^{-1} = \left\{ \int_0^\infty \Delta \varepsilon_{e/h}(t) dt \right\}^{-1} \tag{18}$$

An item of note about the relaxation rates of excited particles in a semiconductor system is the energy gap law for semiconductors: [33]

$$k \approx k_0 e^{-\alpha \Delta E} \tag{19}$$

where ΔE is an energy difference between a charge carrier's initial excitation and the HOMO-LUMO gap. This law describes the expectation that nonradiative relaxations in semiconductors that occur from orbitals closer to the HOMO-LUMO gap will have shorter relaxation times than relaxations that start further from the HOMO-LUMO gap. This expected trend has a positive exponential behaviour.

To find how charge distribution changes during nonradiative relaxation, we need to have our total electron and hole density of the system. This can be found by summing over the density contributions of each KS state for electron and holes, respectively:

$$\rho^{e}(r,t) = \sum_{i>LU} \rho_{ii}^{e}(t) \varphi_{i}^{KS*} \varphi_{i}^{KS*}$$
 (20)

$$\rho^{h}(r,t) = \sum_{i < HO} \rho_{ii}^{h}(t) \varphi_{i}^{KS*} \varphi_{i}^{KS*}$$
 (21)

From here, we can find the current in a system for a given time step by taking the partial derivative of the charge density with respect to time and then integrating over space: [10]

$$j(z,t) = \int_0^z dz' \left[\frac{\partial \rho(z',t)}{\partial t} \right]$$
 (22)

Since current depends on direction, we choose to focus on how the current changes with respect to one dimension (Z). After the current is calculated for each time step of the relaxation, we can find the net charge transfer of the entire relaxation process by integrating, with respect to time, the partial derivative of the current, with respect to position:

$$\rho(z,t) = \int_0^t dt' \left[\frac{\partial j(z,t')}{\partial z} \right]$$
 (23)

Computational and atomistic details

The Janus-like models in our study were composed of near spherical NCs of Pb₆₈Se₆₈ and Cd₃₃Se₃₃. Both NCs are intrinsic semiconductors. The individual NC models were both obtained by cutting nearly spherical structures from a periodic bulk material. The bulk material model was imported from an online database [36]. The near spherical shape cut was chosen since typical PbSe and CdSe NCs in experiments tend to form spherical-like structures [1,3].

After cutting our NC models from the bulk material, we implemented DFT calculations with Vienna Ab initio Simulation Package (VASP) [37]. We geometrically optimised the respective NCs to identify their ground state properties such as band gap (Equation (1)) and partial charge densities of the KS orbitals.

To construct the Janus-like models, we took one of each geometrically optimised NC and placed them in a unit simulation cell with a fixed initial distance between their closest points of contact. One model had 2 Å of spatial displacement. The second model had 4 Å of spatial displacement between QDs. We then geometrically optimised the respective models until the system reached a given energy minimisation tolerance of 10^{-4} eV. The first model remained in close enough contact to have

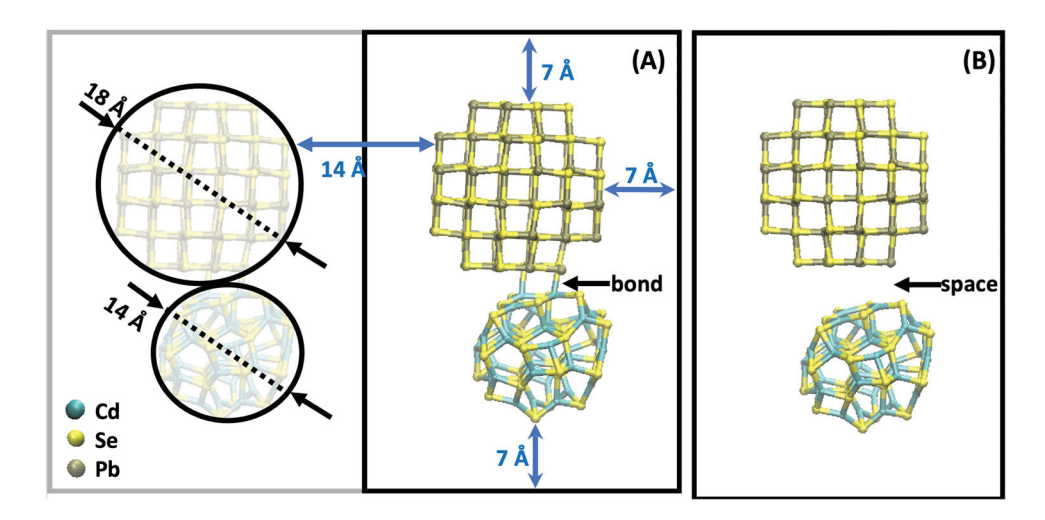


Figure 1. The through-bond (TB) (A) and through-space (TS) (B) Janus-like models for 8 Å of vacuum spacing between QD replicas. Both models are composed of two nanocrystals (NCs) of stoichiometry $Cd_{33}Se_{33} + Pb_{68}Se_{68}$. There is an approximate spacing of 2 Å between the closest contact points of the NCs of the TB model. There is an approximate spacing of 4 Å between the closest NC points for the TS model. Bonds within 3 Å of length are shown in the models. A QD replica of the TB model is shown to the left of (A) to demonstrate total vacuum spacing between QD replicas.

bond formation, so we used it as our 'TB model' test case (Figure 1(a)). This method of fusing simulated QDs via geometry optimisation has been performed in another ab initio study [20]. The second model continued to have a ~4 Å spatial difference of close contact and had no observed bond formation between the NCs, so it was set as our 'TS model' case (Figure 1(b)). The final dimensions of both models are approximately $16 \times 17 \times 29$ Å³ for the TB model, and $16 \times 17 \times 31$ Å³ for the TS model. The geometry optimised models were then examined for band gap and partial charge densities.

The VASP DFT simulations of the individual NCs and Janus-like models were implemented with the GGA-PBE functional [38], on account of the functional's computational efficiency. We used the projected augmented wave (PAW) potentials plane wave basis state to simulate the elements of our model [39].

Electronic structure calculations with VASP software are based on the concept of periodic simulation cells. In order to simulate isolated QDs, sufficient vacuum spacing between the model and the periodic cell boundary is required. For our study, static observables and absorption spectra were calculated for models simulated with 8 Å of vacuum spacing between QD replicas.

To visualise our models, we primarily used Visual Molecular Dynamics (VMD) software [40]. We used a parameter of 3 Å to visualise the bonds forming between ions in the Janus-like models. We also used VMD to visualise the KS partial charge density plots for different KS orbitals. Some supplemental figures were generated using JMOL software [41].

The absorption spectra (Equation (5)) of our models were calculated by inputting the oscillator strength values from the geometry optimised VASP output.

To prepare our system for molecular dynamic calculations, we applied the Nosé-Hoover thermostat (NVT) at 300 K [42]. We then performed molecular dynamics in VASP for 1000 fs [43].

The MD output was then fed into programs designed to calculate NAC (Equation (6)). The overlap functions were calculated for time steps 100-555 fs, which was inclusive of the time span where relaxation occurred for excited electrons and holes. We then calculated the autocorrelation function (Equation (7)) and Redfield tensor (Equation (10)) from the NAC data.

Once we had the Redfield tensor, we could calculate the expectation value of the energy (Equation (17)) and change in charge density over time during the nonradiative relaxation process. We logged the values of the relaxation rates (Equation (18)) for all possible electron and hole particle excitations that had numerically stable solutions. Solutions were deemed numerically unstable if their population dynamics contained numerical artefacts like exceeding the expected normalised occupation range.

For our Janus-like models, we also calculated the change in current (Equation (22)) and net charge transfer (Equation (23)) for a sampling of electron-hole pair initial excitations which had the highest oscillator strengths. Since the NCs in the Janus-like models were displaced with respect to each other along the z-axis dimension, we used the 'z' dimension to analyse the current of the models.

Table 1. Band gap energies, Fermi energy (mid-band gap energy), and total system energies of the individual CdSe and PbSe NCs, and the TB and TS Janus-like models for 8 Å vacuum spacing between QD replicas.

Ground State Observable Data			
Models	Band Gap Energy (eV)	Fermi Energy at Band Gap (eV)	Total System Energy (eV)
Cd ₃₃ Se ₃₃	1.56	-3.44	-158.87
Pb ₆₈ Se ₆₈	1.15	-1.66	-536.47
TB Janus-like	0.90	-2.42	-695.72
TS Janus-like	0.65	-2.56	-695.38

Results

Ground state results

Our DFT calculations gave us information about the ground state of the individual CdSe, PbSe NCs and of both Janus-like models. We obtained the band gap energy, Fermi energy at band gap, and total system energies for our Janus-like models (Table 1).

We found that the band gaps of the Janus-like models were smaller than the individual NC counterparts. This occurs since the CdSe NC conduction band (CB), or LUMO, acts as the CB in the Janus-like model. Meanwhile, the PbSe NC valence band (VB), or HOMO, becomes the VB for the Janus-like model. We see evidence of this relocation of CB and VB by examining the KS orbital partial charge density plots of the Janus-like model (Figure 2).

The newly formed CB and VB in the Janus-like models are closer in proximity than their individual NC components, which results in a smaller band gap. This tradeoff occurs because the relative energy levels of the CdSe VB is lower in energy than the PbSe VB, and the relative energy level of the PbSe CB is higher than the CdSe VB. The shift in the relative Fermi energy (or mid-gap energy level between HOMO and LUMO) for the Janus-like models is a consequence of this as well (Table 1). The stated band gap structure observations are visually summarised in Figure 3.

An important result of the reorganised electronic structure in the Janus-like models is that the CdSe (CB) part of the Janus-like model acts as an electron acceptor, and the PbSe (VB) acts as an electron donor. As a consequence, the lowest excited state of the system, or HOMO -> LUMO transition, is expected to have a charge transfer character when we move on to dynamic observations.

One difference between the ground state of the TB and TS model is that the band gap of the TS model is smaller than the TB model band gap (Table 1). We hypothesise that this slightly smaller band charge may

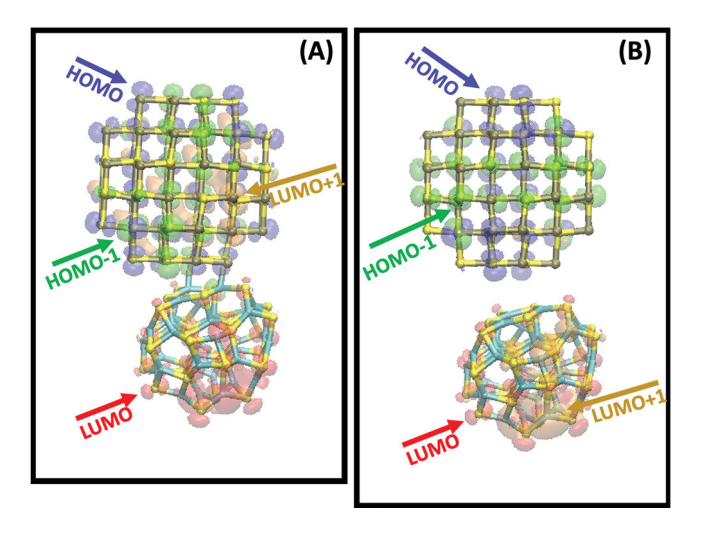


Figure 2. Kohn-Sham (KS) partial charge density plots for the ground state TB (A) and TS (B) Janus-like models. The solid contour surfaces represent charge densities for a particular KS orbital. For both models, the orange contour surface represents the LUMO + 1, the red represents the lowest unoccupied molecular orbital (LUMO), blue represents the highest occupied (HOMO) orbital molecular orbital, and green represents HOMO-1. HOMO-1 and HOMO are composed of Selenium p-atomic orbitals at PbSe for both models. LUMO are composed of Selenium atomic orbitals at CdSe for both models. LUMO + 1 is composes of Pb atomis orbitals for TB model and of Cd atomic orbitals for TS model.

be correlated with the TS model having charge localisation on the CdSe (CB) for LUMO and LUMO + 1 states (Figure 2(b)). In comparison, the TB model LUMO + 1state localises mostly on the PbSe (Figure 2(a)). We hypothesise that this observed difference in localisation of the LUMO + 1 charge distribution for the TB and TS model is a consequence of a perturbation exerted to the whole model by the formation of a bond between the NCs.

The total ground state system energies for the TB and TS models is similar, with the TS model having the slightly more stable configuration (Table 1). Since both energies are comparable, the TS or TB connection has little effect on the total ground state energy.

After analysing the ground state, we calculated the absorption spectra of the simulated geometry optimised models for the Janus-like models and reference QD models. The second lowest peaks of the Janus-like models coincide with the lowest excitation peak of the PbSe QD. These energy transitions are expected to be neutral, with no electric charge. However, the lowest excitation peaks for the Janus-like models are expected to have a charge transfer character and exhibit a lower intensity. The absorption spectra of the Janus-like models are red-shifted compared to their NC counterparts, which is expected since there is a smaller band gap structure.



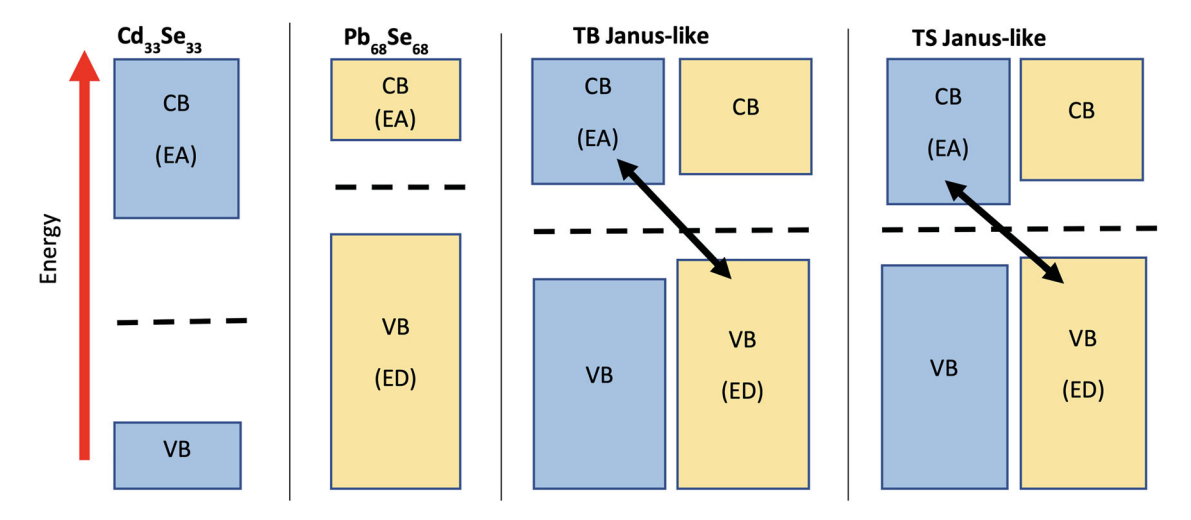


Figure 3. Band gap schematic of the individual NCs and Janus-like models. The black, dashed lines represent the location of the Fermi level energy within the band gap of each model. The relative position of the Fermi energy level and the sizes of the band gap are qualitative representations based on the numerical values found in Table 1. The arrows between certain parts of the conduction band (CB) and valence band (VB) of the Janus-like models' NCs emphasise which parts of the CdSe and PbSe interface are electron donors (ED) and electron acceptors (EA).

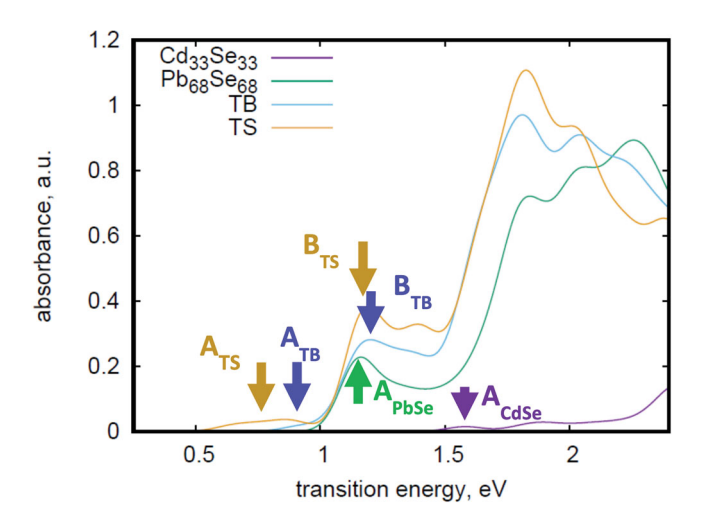


Figure 4. The simulated absorption spectra of the geometrically optimised models. The spectral lines falling off above 3 eV (not shown) occur due to the limited number of calculated transitions states. The lowest peak for each model is labelled as A, second lowest as B. The second lowest peaks in both TB and TS models have a transition energy close to the one for the standalone PbSe QDs. One may attribute these peaks to neutral transitions without charge transfer. The lowest peaks in both TB and TS models have no analogs in standalone QD models. These excitations are expected to have charge transfer character and demonstrate lower intensity.

Dynamics results

We calculated the Redfield Tensor for the Janus-like models and then analysed the dynamics predicted by our Redfield Tensor (Equation (10)), which informed us about the nonradiative dynamics of the system (Equation (11); Figure S1). We first examined the energy relaxation rates

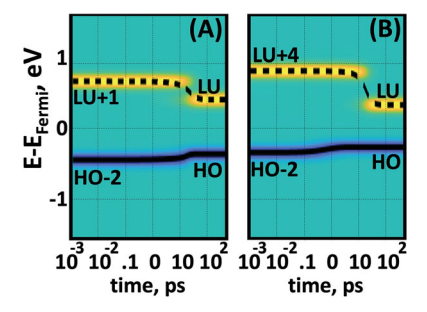


Figure 5. Electron and hole energy relaxation rates for the (A) TB and (B) TS model, for the transitions with each model's respective highest oscillator strength. The black dashed line represents the expectation value of the energy of the electron as it relaxes from some initial orbital above LUMO to LUMO (LU in figure). The black solid line represents the expectation value of the energy of the hole as it relaxes from some initial orbital below HOMO to HOMO (HO in figure). The bright yellow colour indicates electron charge. The dark blue colour shows hole charge. The light blue indicates neutral charge.

for all the numerically stable hole and electron excitations in the Janus-like models. As time passes after an initial excitation, charge carriers dissipate energy into a heat bath. We can calculate (Equation (17)) and plot this energy change and relaxation rate (Equation (18)). An example of these energy trajectories for an electron-hole excitation pair undergoing nonradiative relaxation is presented in Figure 5 for both the TB (Figure 5(a)) and TS model (Figure 5(b)).

The initial excitation for certain electron-hole pairs of the respective models in Figure 5 was selected since they correspond to the highest oscillator strength, indicating that their excitation from ground state has the

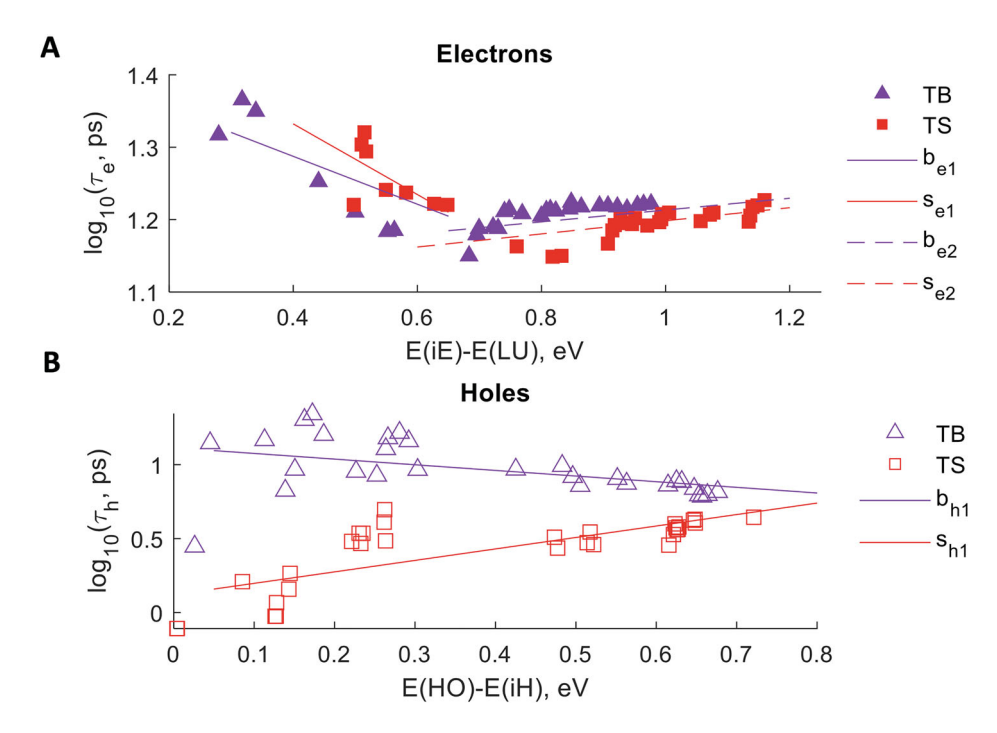


Figure 6. The dependance of the relaxation rates on the energy difference of the (A) electrons initial position (iE) and LUMO. For (B) holes, this dependance is between an initial position (iH) and HOMO. We calculated lines of fit for the behaviour trends of the TB and TS models. Values for the lines of best fit listed in the key are available in Supplemental Information 2.

greatest likelihood of occurring if irradiated. The transition energy for the initial electron–hole pairs are 1.20 and 1.17 eV, respectively. Both of these excitations occur in the infrared range of excitations.

From examining Figure 5, we observe that the expectation value of the energy trajectory shows that the hole charge carriers in both models relax sooner than the electrons. We hypothesise that this occurs since the HOMO charge distribution is more uniformly spread on the PbSe NC, while the LUMO charge is localised further from the HOMO–LUMO gap (Figure 2). Therefore, excited electrons in the CdSe (the VB) have more of a charge and space difference to traverse to before relaxing back to the HOMO–LUMO gap than the holes in the PbSe NC (CB). Additionally, a greater overlap of KS orbitals results in longer relaxation times.

To compare the effect of TB versus TS connection, we calculated the relaxation rates for all charge carrier excitations that came from numerically stable results for both models. We plotted the relaxation rates against the energy difference of the initial charge carrier energy level to its relaxed energy level (Figure 6). We noticed an interesting change in the data trend for the electrons (Figure 6(a)) for both Janus-like models around \sim 0.6–0.7 eV. At energies prior to this behaviour change point, the relaxation times decrease for increasing excitation energy. After the behaviour change point, the models behave according to energy gap law of semiconductors (Equation (19)).

The observed trend of the electrons in both models is likely due to (1) the electron density residing on the PbSe NC for orbitals closer to the LUMO. The LUMO orbital is localised on the CdSe NC, so it initially takes more time for the charge to move through space to LUMO. (2) The electron density for orbitals further from LUMO tends to localise on the same CdSe NC as the LUMO. This allows for quicker electron relaxation times beyond $\sim\!0.7\,{\rm eV}$ (Figure S2).

While the electron excitations are comparable for both models, the hole behaviour is different. As shown in Figure 6(b), the TS model follows the energy gap law of semiconductors. However, the TB model exhibits the opposite trend. Based on hole density graphs, it appears that the TB model has less hole density localisation on the PbSe NC compared to the TS model for initial hole excitations close to HOMO. (Figure S3). This more global spread of charge on the PbSe in the TB model results in hole relaxation taking more time. As the initial hole excitation occurs further from HOMO, the hole charge begins localising in a manner comparable to the TB model, which reduces the relaxation time and causes it to converge with the TS relaxation time values. Consequentially, a trend opposite of the energy gap law occurs when there is a TB connection between the two NCs.

We calculated trendlines for our data in Figure 6 to help quantify the trend. The equations are available in Supplemental Information 2.

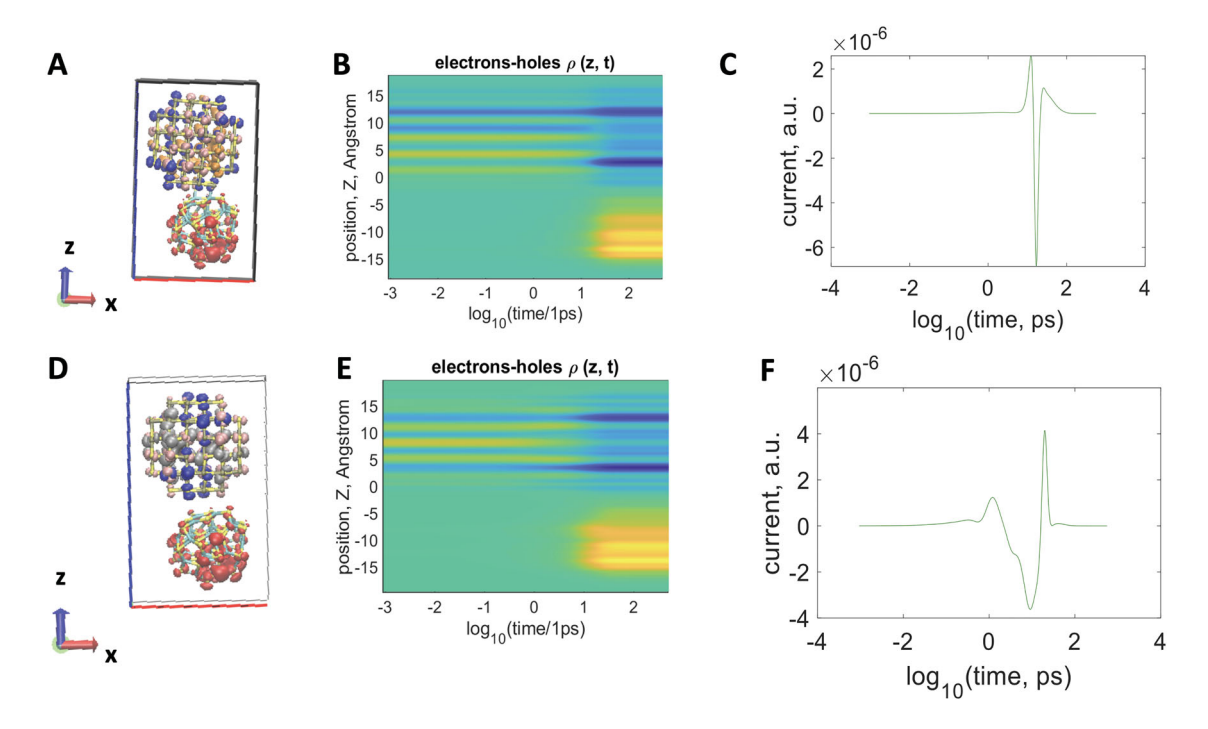


Figure 7. Charge density changes over time as electrons and holes undergo nonradiative relaxation. The TB model (Figures A, B, C) and TS model (Figures D, E, F) dynamics shown are for the same initial hole and electron excitation pairs given in Figure 5. We have (A, D) KS orbital visualisations of the initial excitation orbitals and HOMO and LUMO. Initial electron excitation LUMO + 1 is orange for the TB model, initial electron excitation LUMO + 4 is grey for the TS model. For both models, LUMO is red, HOMO is blue, and initial hole excitation HOMO-2 is pink. For the dynamics, (B, E) we can see how the charge carrier density changes over time with respect to the z-dimension. (C, F). In the contour plots, yellow indicates electron charge density. Dark blue indicates hole charge density. Light green is neutral charge. A time derivative of the charge density at each time step in (B, D) yields a value for the current at each time step in the z-dimension (Equation (22)).

As we calculated the charge carrier relaxation rates, we also calculated how electron and hole densities simultaneously changed over time with respect to the z-dimension of our model (Equations (20, 21)). We then calculated the current (Equation (22)) during the nonradiative relaxation process. A sample visualisation of these results for the TB and TS case is given in Figure 7. The same electron–hole excitations used to produce the data in Figure 5 are used in Figure 7.

The KS partial charge densities for HOMO, LUMO and the state the charge carrier is excited to are represented in Figures 7(a,d). These plots serve as a check to indicate where we expect the charge density of electrons and holes to be when the initial excitation starts and where they should be once they relax to HOMO and LUMO (Figure 2). We created contour plots which show the difference between electron and hole charge densities for the models (Figure 7(b,e)). The yellow contours represent electron charge density, and the dark blue contours represent hole charge density. The charge density is evaluated with respect to the z-dimension, which matched the axis that our NCs were separated across. The current during the nonradiative relaxation process is presented in

Figure 7(c,f). The current undergoes the greatest change when the relaxation to HOMO-LUMO occurs.

We can observe in both Janus-like models that there is some exchange of negative charge (electrons) with respect to the spatial localisation. The relaxed state of the system shows that the electrons reside on the CdSe NC, which is LUMO. The holes remain on the PbSe NC, which has HOMO and the HOMO-2 orbital. The lowest excitation of both models is a charge transfer from CdSe to PbSe. However, charge transfer dynamics do depend on whether there is a bond connection in space, as indicated by the different evolutions of the current in the Z-dimension for the TB and TS case (Figure 7(e,f)).

Since the current depends on the choice of model, we went ahead to calculate the numerical net charge of the entire nonradiative relaxation process. We selected a sample of the 18 highest numerically stable oscillator strength electron-hole excitations for the TB model and a sample of 19 for the TS model. To obtain the net charge density change, we enter the current (Equation (22)) calculated for a given electron-hole excitation pair into Equation (23). The pair choice was important here since the overall charge transfer depends on changes in

electron and hole density. The chosen pairs are listed in Supplemental Tables S1 and S2.

The resulting numerical net charge transfers for the given sample are presented in Figure 8. We found that both the TB and TS models tended to have a net negative charge transfer. For the electron density case shown in Figure 7(b,e), this makes sense since the electrons relax from the PbSe NC to the CdSe for the given examples. However, as shown in Figure 8, the TB model exhibited some positive net charge transfer. Our investigations of comparing the TB and TS models' ground state electronic structure (Figure 2) and the dynamic hole nonradiative relaxation rates (Figure 6) show that having a bond alters the electronic configuration and dynamics of the Janus-like model. Therefore, we expect the TB model to allow for some differing net change in charge transfer for different electron-hole excitation pairs.

Discussion

The focus of our research was to prove that properties related to charge transfer across an interface for Januslike QDs are impacted by having a TB or TS connection. From our ground state results, we found that the band gap of the static TS model was smaller than the TB model. The value of the band gap energy is a consequence of the electron-hole attraction between the orbitals across the interface of the NCs. Both models had comparable total ground state energy (Table 1). To gain insight into why the TB and TS model band gaps differed, we went on to examine the KS partial charge density orbital configurations for KS orbitals near the HOMO and LUMO (Figure 2). We determined that band gap difference may be correlated to the LUMO + 1 orbital charge density localising on the PbSe NC in the TB model. The TS model LUMO + 1, in comparison, localised on the CdSe. The bond connection therefore affects the static electronic structure.

From our absorption spectra, we observed that both TB and TS models had lower energy, red-shifted peaks. This indicates a charge transfer character is expected for these lower energy transitions.

For our Redfield Tensor, we observed that the hole nonradiative relaxation rate of the TS model followed the energy gap law, while the TB model followed an opposite trend (Figure 6(b)). We determined that the TB model had a slower relaxation rate for initial hole excitations near HOMO since the hole charge density distribution is less localised on the PbSe NC in comparison to the TS model. The hole charge distributions for initial excitations much further from HOMO become comparable for the TB and TS cases, which results in a convergence

of their relaxation trends. The longer relaxation time for holes can be useful if one needs to harvest charge carriers, therefore, it is a beneficial charge transfer property for solar cells.

The effect of a bond connection was also evident from examining net charge transfer during the nonradiative relaxation process (Figure 8). For the sampled excitation pairs, both TB and TS models tended to have a net negative charge transfer overall. However, the TB model had some cases of net positive charge. We expected there to be some qualitative difference in the net charge since the TB model has a different electronic structure for LUMO $+\,1$ in the ground state and different hole relaxation rates for the excited state. Therefore, we were able to prove that having a TB or TS connection between the interface of the NCs in Janus-like QD does affect charge transfer properties.

If we were to compare our results to experimental systems, some factors in our simulated approach must be considered. For example, our individual NCs and Januslike models were simulated with VASP in a vacuum space of approximately 8 Å vacuum spacing between QD replicas. As a consequence, all models are not simulated in unit cells of the same size. For example, in the 8 Å case, meaning that there are 4 Å of vacuum between the model and each of the periodic boundaries of the cell (Figure 1), the unit cell sizes ranged from $\sim\!20\times22\times20$ for the CdSe NC to $\sim\!24\times25\times39$ for the TS Janus-like model. A more rigorous comparison of the four QD models could be undertaken if all unit cell sizes matched. However, we still expect similar qualitative trends to occur for our observables.

Additionally, experiments usually have a medium interacting with the interface of QD models, instead of a vacuum. These experiments show that the choice of medium between the NCs has an effect on charge transfer across the interface [17]. The influence of a surrounding solvent or solid matrix results in a polarisation correction to Coulomb interactions. Polarisation can be taken into account by doing the following: (1) having a vacuum in zeroth order, which was done in this study. (2) Explicit modelling of surrounding molecules. (3) Polarised continuum medium. (4) Polarisation correction in many body perturbation theory [44,45].

Our simulated Janus-like QDs are sizes $16 \times 17 \times 29$ ų (TB model) and $16 \times 19 \times 31$ ų (TS model), which would have the same volume as a spherical particle with a diameter of at most 24 Å. Some experiments have synthesised QDs with radii ranging from 40 to 70 Å, [46] or 45 Å [17]. We chose to simulate QDs with smaller radii since the critical importance of QD radius originates from comparing it to the Bohr radius of an exciton for a given material. For our QDs materials, $a_{Bohr}^{PbSe} = 4.60$ Å and

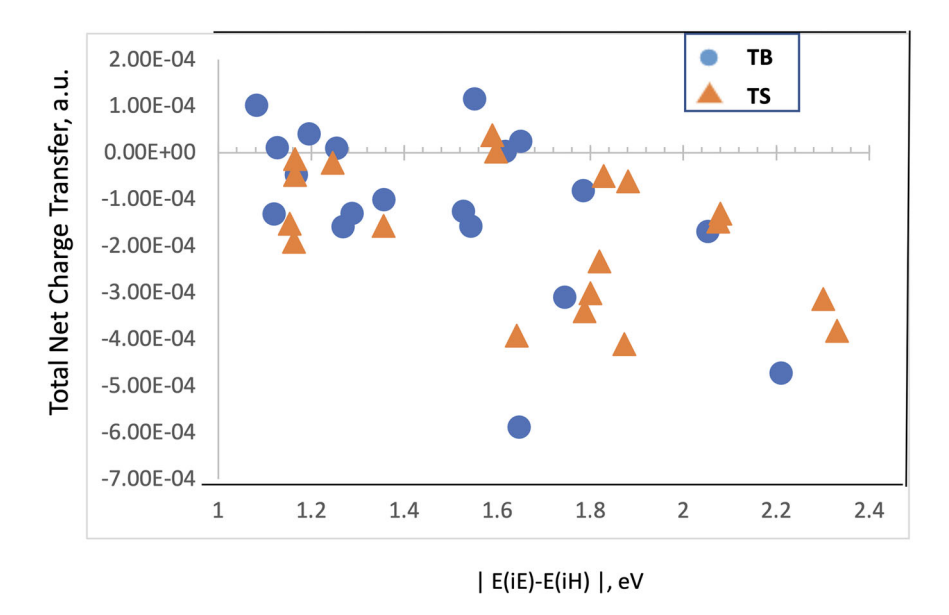


Figure 8. Net charge transfer (Equation (22)). in the z-dimension as function of initial excitation for a sample of different initial electron exitation (iE) and initial hole excitation (iH) combinations which had the highest oscillator strengths (Tables S1 and S2).

 $a_{Bohr}^{CdSe} = 5.40$ Å. Consequentially, any spherical QD with a radius less than 2 Bohr exciton radius will show the same qualitative properties dictated by quantum confinement rather than electron–hole interactions in a range of $0 < r < r_{Bohr}$. The gap systematically scales as a function of dot size related to particle-in-spherical-box scaling. Our studied models fit in this range.

Some ab initio and experimental studies also give motivation for our QD choice size. Ab initio studies on CdSe and PbSe NCs have shown that small, stoichiometric 'magic' QDs with sizes comparable to our study can simulate bulk material properties [47]. Experimentalist have synthesised NCs of this size for our chosen stoichiometry of Cd₃₃Se₃₃ [16,48]. They have also synthesised PbSe QDs as small as 10 Å in diameter [49], which is smaller than our estimated Pb₆₈Se₆₈ diameter of roughly 15 Å. These cited experimental studies tended to focus on the synthesis of QDs, with the exception of the study on the synthesis and fluorescence quantum yield of 'magic sized' PbSe QDs. While the PbSe study identified excitonic emission from cluster and surface states as the source of emission, the physical explanation of why there was such high quantum yield was that the quantum confinement effect was responsible. Relaxation channels such as nonradiative relaxation or relaxation in the intraband were unexplored. Regardless, these experimental studies on magic sized QDs are useful to the computation community because magic-sized QDs are more accessible for ab initio studies. This accessibility allows for a greater potential of comparable experimental and theoretical results for analysis. Ab initio studies are useful for the experimental community because the femtosecond monitoring of the dynamics of the photoexcited states is often performed in a blind way, especially in systems with substantial influence of surface effects. The dynamics of charge and energy transfer through the interface of two semiconductor nanostructures from this work provide a reference point in the interpretation of the femtosecond experiments.

Smaller sized models, as well as smaller vacuum size, are also advantageous for the NAC process used in this work. Authors have developed an original method for excited state analysis and dynamics induced by interaction with lattice vibrations. The electron phonon couplings used to parameterise the Redfield tensor need to have a reconfiguration of electronic structures multiple times at a range of interatomic displacement for phonon normal modes along the MD trajectory. The NAC and MD methods are computationally expensive, but doable. However, a simultaneous account of both effects takes place: formation of bound excitons and nonadiabatic dynamics have a numerical expense and scaling much higher than each of the individual methods. This scaling can reach three orders of magnitude higher than the typical calculation. Analysis of electronic structure and dynamics must be done at the same level for consistency, as it is practiced in this work.

The smaller size chosen for our QDs may bring into question the effect of surface states on our system. While it is true that the relative number surface states increase as QD size decreases, the *ab initio* studies of the surface of CdSe have shown that the surface is self-healing [50]. PbSe has also been shown to less susceptible to surface effects than CdSe [51]. Our research will eventually have

QDs smashed together with a larger surface area of interaction. The current model with the smaller surface area interaction allows us to identify contributions from the individuals NC subsystems. It also allows us to treat these influences in a perturbative manner. Studies on surface states with a greater surface area have been done previously for in PbS | CdS Janus QDs 3 and for PbSe | CdSe core–shell QDs [13,17,18].

The effect of passivation on the surface of the QDs may also be in question. Previous studies Cd₃₃Se₃₃ QDs have shown that stoichiometric 'magic QDs' are less sensitive to passivation than their nonstoichiometric counterparts. This study also examined the case of Cd₃₃Se₃₃ attached to neutral ligands, such as such as amines and phosphine oxides (OPMe₃), and found that surface reconstructions in polar solvents partially suppressed ligand-associated defects [52]. The reader is invited to observe surface reconstruction of PbSe CdSe QDs in comparison to the original fragment carved from the bulk structure. The reader is also invited to focus on work by Kilina et al. [53] and identify surface reconstructions of the models used in that paper compared to fragments of the unperturbed bulk. The fragments of unperturbed bulk exhibit undercoordinated surface atoms of Pb, Se, Cd, which contribute dangling bonds to the gap and would need passivation by ligands such as Tri-octyl-phosphine (TOP) and trioctylphosphine oxide (TOPO), the latter of which has been used in ab initio studies of surface passivation on Cd₃₃Se₃₃ NCs [54]. However, surface reconstruction compensates for these dangling bonds. Another ab initio study suggests that using hydrogen passivation on CdSe QDs would increase the band gap of the structure [55].

An analysis of larger QDs would be applicable if one were interested in scanning the relative sizes of PbSe and CdSe dots to explore a mutual gap for engineering charge transfer direction. Larger size dots may also be of interest for exploring polaron formation.

We chose to apply the PBE functional for our DFT calculations. While this functional is computationally efficient, it is well known that it underestimate the energy gap for semiconductors [56]. Therefore, the band gap values should be evaluated in a more qualitative manner. Choosing to use pure functionals instead of hybrid functionals is known to introduce a systematic error into NAC calculations [57]. Therefore, qualitative trends should be focused on over quantitative trends in our dynamics results as well.

We also had to consider if the Van der Waals interaction between the NCs in the TB and TS models affected the bang gaps [58]. When two NCs are near each other, a Van der Waal interaction between the interface can create an attractive force that reduces the band gap. We calculated geometry optimisations in VASP where the Van

der Waals interaction parameter was included. The percentage difference in energy band gap with and without the Van der Waals interaction had a max of 3% for both models. Therefore, we determined that the Van der Waals interaction has a minimal effect on our results.

A correction that could have been made to our results would be involving spin orbit coupling (SOC) in order to account for the heavier nature of the Pb element in the Janus-like models. Involving SOC would reduce the band gap of our electronic structure. However, we expect that the qualitative behaviour of our ground states and relaxation rates would be similar, based on computational simulations that considered SOC while simulating materials with Cd and Se [59]. The inclusion of SOC effects is planned for future calculations.

Since our dynamic results are based on DFT calculations, there may be some question as to how our results will be affected by interactions including excited states, long-range bonding, Coulombic interactions, and charge transfer excitations. Excited state analysis based on DFT calculations has been done in previous work by applying many-body perturbation theory [44,45] and will be applied in future work with more complex models. In the present work, these excited state corrections may be omitted since the main focus is on the picosecond-range rates of cooling of hot charge carriers, which is affected by the values of intraband subgaps and offsets. The excited state corrections would modify the interband gap, which affects the nanosecond range recombination, which is beyond the focus of this work. Additionally, the results of an ab initio study [54] suggest that for bare, unpassivated QD such as Cd₃₃Se₃₃, correlation effects are not very significant. Correlation effects are closely related to excitonic effects. An ab initio study of the absorption spectra of Cd₃₃Se₃₃ showed that applying an uncorrelated, single-particle KS approach (B3LYP functional) red-shifted the spectrum by $\sim 0.34\,\mathrm{eV}$ in comparison to a correlated time-dependent DFT calculation (TDB3LYP functional) approach. There was minimal change to the overall spectrum line shape. We therefore propose that our bare, Janus-like QDs will also experience qualitatively similar results to results involving excited state effects.

Incorporating long-range interaction effects on DFT calculations are beyond the scope of this paper. If one is interested applying them, correction functionals such as CAM_B3LYP [60] are available. A more thorough treatment of the Van der Waal interaction is available as well [61]. Regarding Coulombic interactions, previous work has shown that this interaction can be considered a small perturbation for small QD systems since the confinement energy of the QD is much larger than the electron–hole Coulomb energy [47]. Previous work has found that our approach incorporates charge transfer effects in an

improved manner [45]. Future work will address these deficiencies in the theory, while the current work informs us about qualitative trends which will serve as a reference point when we proceed to more complex models. One may explore the effects of introducing defects into larger models as well [62].

The selection of methods is based on recognition of the numerical cost of nonadiabatic dynamics combined with excited state treatment is orders of magnitude higher than nonadiabatic dynamics in the basis of non-interacting orbitals. The main strength of this work and its significance to the community is in the domain of addressing dynamical aspects of photoexcitation facilitated by interaction of electronic degrees of freedom with nuclear degrees of freedom. See Figure S4 for a visualisation of how the ionic positions change during the course of the MD trajectory. Refer to Figure S5 to see how the KS orbital energies change during the MD trajectory.

The challenge of addressing dynamical aspects is of additional degree of complication compared to addressing of excited states. Tools for addressing nonadiabatic dynamics slowly infiltrate into the public domain of software but are not yet available to the needed degree.

Conclusions

QDs have been experimentally and computationally shown to have beneficial charge transfer properties for photogenerated carriers such as tunable band alignment and MEG. To contribute to this understanding, we simulated two Janus-like heterostructure QDs composed of Pb₆₈Se₆₈ + Cd₃₃Se₃₃ NCs, one with a TB connection between the spherical-like NCs, and one with a TS connection. Our purpose was to prove that having a bond connection between the interfaces of the NCs would impact the charge carrier dynamics.

To carry out this investigation, we compared the simulated ground state properties of our Janus-like models and their individual NCs by applying DFT. We calculated static observables and absorption spectra. We found that the band gaps for the Janus-like models were smaller than the respective individual NCs (Table 1). In the Janus-like models, the CdSe NC acted as the LUMO, or CB. The PbSe acted as the HOMO, or VB (Figure 3). As a result, we expect that the lowest excited state of Janus-like systems will have a charge transfer character when we analyse the dynamics of the system. Our observations of the absorption spectrum show evidence of this as well due to the low transition energy and intensity of the initial absorption peaks for the Janus-like models (Figure 4).

We also saw that the LUMO orbital localised on the same PbSe NC as the HOMO. In comparison, the TS model LUMO was localised on the same CdSe NC as the

LUMO. We concluded that the bond connection between the interfaces altered the electronic structure near the energy band gap.

We then performed MD and then calculated on-thefly NAC for the trajectory of our Janus-like models. The NACs were used to create the Redfield tensor, which informed us about the charge carrier dynamics of our system due to nonradiative relaxation.

We calculated the relaxation rates from different initial charge carrier excitation orbitals to the HOMO–LUMO gap. We compared the relaxation rates to the energy difference of the excitation and ground state (Figure 6). Electron charge carriers (Figure 6(a)) in both Janus-like models exhibited an abrupt change in relaxation rate for excitation energy of a carrier around 0.6–0.8 eV. After the behaviour change point, the electron relaxation rates followed the energy gap law of semiconductors. Prior to this point, the electron relaxation rate followed an opposite trend: the nonradiative relaxation times decreased exponentially for increasing energy.

A difference between the TB and TS models was evident when we examined the hole relaxations in the VB (Figure 6(b)). The TB model relaxation rates followed the energy gap law. The TS model had an opposite trend: its relaxation times decreased exponentially for increasing energy difference in excitation. This differing behaviour in the TB model is due to the hole charge density having a more global spread of charge on the PbSe NC for KS orbitals near HOMO (Figure S3). If one needs to harvest charge carriers near LUMO after excitation has occurred, the long relaxation time exhibited in the TB model would be useful for charge transfer.

We also calculated the net change in charge carrier density as the system relaxed with respect to the z-dimension, or the dimension corresponding to the physical displacement of our NCs. The numerically evaluated net charge showed that the TB and TS models both favour net negative values (Figure 8). The TB model, however, yielded some positive net charge values. We expected some qualitative difference would occur since we already proved that the ground state electronic configuration and hole relaxation rates for the TB and TS models differed.

Since our dynamic results did not include excited state calculations, they represent qualitative trends that we would expect to see replicated in calculations involving such effects.

In summary, we found that both Janus-like models had a smaller bandgap than their individual NC counterparts, which is useful for charge transfer. The simulated absorption spectra also give evidence for charge transfer. We determined that having a bond connection through the interface does affect the charge carrier dynamics. Having a TB connection altered the ground state electronic



structure for LUMO + 1 and altered the hole nonradiative relaxation rates. Notably, relaxation times of holes near LUMO are longer for the TB than the TS model. Our numerical evaluation of a net current across the interface showed that net charge transfer in the TB model could be positive or negative for a given sample. Therefore, we conclude that having a TB versus TS connection for Janus-like particles will affect their charge transfer capabilities.

The results of this work are expected to contribute to ongoing exploration of coupling between separated quantum dots [63].

Acknowledgements

We also acknowledge that this research used resources of the National Energy Research Scientific Computing Center (NERSC), a U.S. Department of Energy Office of Science User Facility located at Lawrence Berkeley National Laboratory, operated under Contract No. DE-AC02-05CH11231, allocation 'Computational Modeling of Photo-catalysis and Photo-induced Charge Transfer Dynamics on Surfaces'. DSK acknowledges the support of NSF CHE-1944921. DSK thanks David Micha, Sergei Tretiak, Oleg Prezhdo, and Svetlana Kilina for inspiring discussions. HG thanks David Graupner, Landon Johnson, Dr. Yulun Han, Dr. Dinesh Thapa, Kamrun Nahar Keya, Patricia Adeoye, Adam Flesche, William Tupa, Joseph Granlie, Amara Arshad, Meade Erickson, Sarah Ghazanfari, and other collaborators for editorial suggestions.

Disclosure statement

No potential conflict of interest was reported by the author(s).

Funding

We gratefully acknowledge the support of the National Science foundation via NSF CHE-2004197 for this study. This work was supported by Chemical Sciences, Geosciences, and Biosciences Division [grant number DE-AC02-05CH11231, allocation Computational Modeling of Photocatalysis and Photoinduced Charge Transfer Dynamics on Surfaces]; National Science Foundation [grant number 1944921].

ORCID

Dmitri S. Kilin http://orcid.org/0000-0001-7847-5549

References

- J. Zhang, B.D. Chernomordik, R.W. Crisp, D.M. Kroupa, J.M. Luther, E.M. Miller, J. Gao and M.C. Beard, ACS Nano. 9, 7151–7163 (2015). doi:10.1021/acsnano.5b01859
- [2] Jeffrey M. Pietryga, Donald J. Werder, Darrick J. Williams, Joanna L. Casson, Richard D. Schaller, Victor I. Klimov, and Jennifer A. Hollingsworth, J. Am. Chem. Soc. 130, 4879–4885 (2008). doi:10.1021/ja710437r
- [3] D.M. Kroupa, G.F. Pach, M. Vörös, F. Giberti, B.D. Chernomordik, R.W. Crisp, A.J. Nozik, J.C. Johnson, R. Singh,

- V.I. Klimov, G. Galli and M.C. Beard, ACS Nano. 12, 10084–10094 (2018). doi:10.1021/acsnano.8b04850
- [4] L. Lystrom, P. Tamukong, D. Mihaylov and S. Kilina, J. Phys. Chem. Lett. 11 (11), 4269–4278 (2020). doi:10.1021/ acs.jpclett.0c00845
- [5] A.L. Efros and L.E. Brus, ACS Nano. 15 (4), 6192–6210 (2021). doi:10.1021/acsnano.1c01399
- [6] A.I. Ekimov, A.L. Efors and A.A. Onushchenko, Solid State Commun. 56 (11), 921–924 (1985). doi:10.1016/S00 38-1098(85)80025-9
- [7] S.K. Matta, T. Liao and S.P. Russo, J. Mater. Sci. Technol. 155, 142–147 (2023). doi:10.1016/j.jmst.2022. 12.076
- [8] M. Bhati, S.A. Ivanov, T.P. Senftle, S. Tretiak and D. Ghosh, J. Mater. Chem. A. 10 (2022). doi:10.1039/D1TA07983B
- [9] A.J. Nozik, Physica E. **14** (1-2), 115–120 (2002). doi:10. 1016/S1386-9477(02)00374-0
- [10] H. Yulun, D.A. Micha and D. Kilin, Mol. Phys. 113 (3-4), 327–335 (2015). doi:10.1080/00268976.2014.944598
- [11] S. Fischer, N.D. Bronstein, J.K. Swabeck, E.M. Chan and A.P. Alivisatos, Nano Lett. **16** (11), 7241–7247 (2016). doi:10.1021/acs.nanolett.6b03683
- [12] J. Cui, Y.E. Panfil, S. Koley, D. Shamalia, N. Waiskopf, S. Remennik, I. Popov, M. Oded and U. Banin, Nat. Commun. 10 (1), 5401 (2019). doi:10.1038/s41467-019-13349-1
- [13] Y. Zhang, Q. Dai, X. Li, B. Zou, Y. Wang and W.W. Yu, J. Nanopart. Res. 13, 3721–3729 (2011). doi:10.1007/s1105 1-011-0293-3
- [14] V.V. Albert, S.A. Ivanov, S. Tretiak and S. Kilina, J. Am. Chem. Soc. 115 (32), 15793–15800 (2011).
- [15] J. Noffsinger, E. Kioupakis, C.G. Van de Walle, S.G. Louie and M.L. Cohen, Phys. Rev. Lett. 108 (16), 167402 (2012). doi:10.1103/PhysRevLett.108.167402
- [16] Y. Wang, Y. Zhang, F. Wang, D.E. Giblin, J. Hoy, H.W. Rhors, R.A. Loomis and W.E. Buhro, Chem. Mater. 26 (7), 2233–2243 (2014). doi:10.1021/cm404068e
- [17] C. Schedel, F. Strauß, K. Kumar, A. Maier, K.M. Wurst, P. Michel and M. Scheele, ACS Appl. Mater. Interfaces. 13 (40), 47954–47961 (2021). doi:10.1021/acsami.1c13581
- [18] N. Yazdani, S. Andermatt, M. Yarema, V. Farto, M.H. Bani-Hashemian, S. Volk, W.M.M. Lin, O. Yarema, M. Luisier and V. Wood, Nat. Commun. 11 (2020). doi:10.1038/s41467-020-16560-7
- [19] N.T. Dandu, S. Kilina and S. Kilin, Chem. Phys. **481**, 144–156 (2016). doi:10.1016/j.chemphys.2016.09.003
- [20] Y. Zhou, C.S. Garoufalis, S. Baskoutas, Z. Zeng and Y. Jia, Nano Lett. 22 (12), 4912–4918 (2022). doi:10.1021/acs.na nolett.2c01459
- [21] H. Ren, Y. Song, R. Yu, M. Tian and L. He, Dyes and Pigm. 204, 110389 (2022). doi:10.1016/j.dyepig.2022.110389.
- [22] J.M. Elward, B. Thallinger and A. Chakraborty, J. Chem. Phys. 28, 124105 (2012). doi:10.1063/1.3693765
- [23] O. Lehtonen and D. Sundholm, J. Chem. Phys. **125** (14) (2006). doi:10.1063/1.2354496
- [24] A. Puzder, A.J. Williamson, J.C. Grossman and G. Galli, Phys. Rev. Lett. 88 (9), 097401 (2002). doi:10.1103/Phys RevLett.88.097401
- [25] M.L.D. Puerto, M.L. Tiago and J.R. Chelikowsky, Phys. Rev. B. 77 (4), 045404 (2008). doi:10.1103/PhysRevB.77. 045404
- [26] S.V. Kilina, D.S. Kilin and O.V. Prezhdo, ACS Nano. 3 (1), 93–99 (2009). doi:10.1021/nn800674n



- [27] C.F. Craig, W.R. Duncan and O.V. Prezhdo, Phys. Rev. Lett. 95 (16), 163001 (2005). doi:10.1103/PhysRevLett.95.
- [28] A.M. Virshup, C. Punwong, T.V. Pogorelov, B.A. Lindquist, C. Ko and T.J. Martínez, J. Phys. Chem. B. 113 (11), 3280-3291 (2009). doi:10.1021/jp8073464
- [29] T.J. Martinez, Acc. Chem. Res. 39 (2), 119-126 (2006). doi:10.1021/ar040202q
- [30] Z. Zhang, J. Wang, Y. Zhang, J. Xu and R. Long, J. Phys. Chem. Lett. 13 (46), 10734–10740 (2022). doi:10.1021/acs.jpclett.2c03097
- [31] P.O. Dral, M. Barbatti and W. Thiel, J. Phys. Chem. Lett. 9 (19), 5660–5663 (2018). doi:10.1021/acs.jpclett.8b02469
- [32] D.J. Vogel and D.S. Kilin, J. Phys. Chem. 119 (50), 27954-27964 (2015). doi:10.1021/acs.jpcc.5b06434
- [33] R. Englman and J. Jortner, Mol. Phys. 18, 145–164 (1970). doi:10.1080/00268977000100171
- [34] P. Hohenberg and W. Kohn, Am. Phys. Soc. 136 (3B), B864-B871 (1964). doi:10.1103/PhysRev.136.B864
- [35] W. Kohn and L.J. Sham, Phys. Rev. 140 (4A), A1133-A1138 (1965). doi:10.1103/PhysRev.140.A1133
- [36] A. Jain, S.P. Ong, G. Hautier, W. Chen, W.D. Richards, S. Dacek, S. Cholia, D. Gunter, D. Skinner, G. Ceder and K.A. Persson, APL Mater. 1 (1, (2013). doi:10.1063/1. 4812323
- [37] G. Kresse and J. Furthmüller, Comput. Mater. Sci. 6 (1), 15-50 (1996). doi:10.1016/0927-0256(96)00008-0
- [38] J.P. Perdew, K. Burke and M. Ernzerhof, Phys. Rev. 78 (7), 1396-1396 (1997). doi:10.1103/PhysRevLett.78.1396
- [39] P.E. Blöchl, Physical Review B. 50 (24), 17953–17979 (1994). G. Kresse and D. Joubert, Phys. Rev. B **59** (3), 17953-17979 (1999). doi:10.1103/PhysRevB.50.17953
- [40] W. Humphrey, A. Dalke and K. Schulten, J. Mol. Graphics. 14, 33–38 (1996). doi:10.1016/0263-7855(96)00018-5
- [41] A. Herraez, How to use Jmol to study and present molecular structures. (Lulu Enterprises, Morrisville, NC, USA, 2007).
- [42] S. Nosé, J. Chem. Phys. **81** (1), 511–519 (1984). doi:10.10 63/1.447334
- [43] D. Marx and J. Hutter, Ab initio molecular dynamics. Basic theory and advanced methods (Cambridge University Press, Cambridge, 2009).
- [44] A. Kryjevski, B. Gifford, S. Kilina and D. Kilin, J. Chem. Phys. 145 (15), 154112 (2016). doi:10.1063/1.4963735
- [45] A. Kryjevski, D. Mihaylov and D. Kilin, J. Phys. Chem. 9 (19), 5759-5764 (2018).

- [46] R.J. Ellingson, M.C. Beard, J.C. Johnson, P. Yu, O.I. Micic, A.J. Nozik, A. Shabaev and A.L. Efros, Nano Lett. 5 (5), 865-871 (2005). doi:10.1021/nl0502672
- [47] S. Kilin, D. Kilin and S. Tretiak, Chem. Rev. 115 (12), 5929-5978 (2015). doi:10.1021/acs.chemrev.5b00012
- [48] A. Kasuya, R. Sivamohan, Y.A. Barnakov, I.M. Dmitruk, T. Nirasawa, V.R. Romanyuk, V. Kumar, S.V. Mamykin, K. Tohji, B. Jeyadevan, K. Shinoda, T. Kudo, O. Terasaki, Z. Liu, R.V. Belosludov, V. Sundararajan and Y. Kawazoe, Nat. Mater. 3 (2), 99-102 (2004). doi:10.1038/nmat1056
- [49] M.E. Christopher, L. Guo, J.J. Peterson, S. Maccagnano-Zacher and T.D. Krauss, Nano Lett. 8 (9), 2896-2899 (2008). doi:10.1021/nl801685a
- [50] A. Puzder, A.J. Williamson, F. Gygi and G. Galli, Phys. Rev. Lett. 92 (21), 217401 (2004). doi:10.1103/PhysRevLet t.92.217401
- [51] F.W. Wise, Acc. Chem. Res. 33 (11), 773–780 (2000). doi:10.1021/ar970220q
- [52] S.V. Kilina, P.K. Tamukong and D.S. Kilin, Acc. Chem. Res. 49 (10), 2127-2135 (2016). doi:10.1021/acs.accounts. 6b00196
- [53] S.V. Kilina, C.F. Craig, D.S. Kilin and O.V. Prezhdo, J. Phys. Chem. C. 111 (12), 4871–4878 (2007). doi:10.1021/ jp0669052
- [54] S. Kilina, S. Ivanov and S. Tretiak, J. Am. Chem. Soc. 131 (22), 7717-7726 (2009). doi:10.1021/ja9005749
- [55] H. Deng, S. Li, J. Li and S. Wei, Physical Review B. **85** (19), 195328 (2012). doi:10.1103/PhysRevB.85.195328
- [56] J.P. Perdew and M. Levy, Phys. Rev. Lett. **51** (20, (1983). doi:10.1103/PhysRevLett.51.1884
- [57] Y. Lin and A.V. Akimov, J. Phys. Chem. A. 120 (45), 9028–9041 (2016). doi:10.1021/acs.jpca.6b09660
- [58] J. Angyan, I. Gerber, A. Salvin and J. Toulouse, Phys. Rev. A. 72 (1, (2005). doi:10.1103/PhysRevA.72.012510
- [59] M. Ribeiro Jr, L.R.C. Fonseca, T. Sadowski and R. Ramprasad, J. Appl. Phys. 111 (7), 073708 (2012). doi:10.1063/1.3699054
- [60] T. Yanai, D.P. Tew and N.C. Handy, Chem. Phys. Lett. 393 (1-3, (2004). doi:10.1016/j.cplett.2004.06.011
- [61] S. Grimme, J. Antony, S. Ehrlich, and H. Krieg, J. Chem. Phys. 132 (15), 154104 (2010). doi:10.1063/1.3382344
- [62] J. Granlie, E. Hobbie, and D. Kilin, J. Phys. Chem. Lett. 14 (26), 6202–6208 (2023). doi:10.1021/acs.jpclett.3c01182
- [63] S. Koley, J. Cui, Y.E. Panfil and U. Banin, Acc. Chem. Res. 54 (5), 1178–1188 (2021). doi:10.1021/acs.accounts. 0c00691